Solid-State Coordination Chemistry: Structural Influences of Copper−Phenanthroline Subunits on Oxovanadium Organophosphonate Phases. Hydrothermal Synthesis and Structural Characterization of the Two-Dimensional Materials $[Cu(phen)(VO)(O_3PCH_2PO_3)(H_2O)]$, $[\{Cu(phen)\}_2(V_2O_5)(O_3PCH_2CH_2PO_3)]$, and $[\{Cu(phen)\}_2(V_3O_5)(O_3PCH_2CH_2CH_2PO_3)_2(H_2O)]$ and of the Three-Dimensional Phase $[\{Cu(phen)\}_2(V_3O_5)(O_3PCH_2PO_3)_2(H_2O)]$

Robert C. Finn,[†] Robert Lam,[‡] John E. Greedan,*[,‡] and Jon Zubieta*[,†]

Department of Chemistry, Syracuse University, Syracuse, New York 13244, and
Department of Chemistry, McMaster University, Hamilton, Ontario, Canada L8S 4M1

Received February 13, 2001

The hydrothermal reactions of $CuCl_2 \cdot 2H_2O$, Na_3VO_4, 1,10-phenanthroline, and the appropriate organodiphosphonate ligand yield $[Cu(phen)(VO)(O_3PCH_2PO_3)(H_2O)]$ (**1**), $[\{Cu(phen)\}_2(V_2O_5)(O_3PCH_2CH_2PO_3)]$ (**2**), $[\{Cu(phen)\}_2(V_3O_5)(O_3PCH_2CH_2CH_2PO_3)_2\ (H_2O)]$ (**3**), and $[\{Cu(phen)\}_2(V_3O_5)(O_3PCH_2PO_3)_2(H_2O)]$ (**4**). Compounds **1**−**3** exhibit two-dimensional structures. The structures exhibit distinct vanadium building blocks: square pyramidal, mononuclear V(IV) sites in **1**, a binuclear unit of corner-sharing V(V) tetrahedra in **2**, and a trinuclear unit of corner-sharing V(V) square pyramids and a V(IV) octahedron in **3**. The network structures of **1** and **2** are constructed from one-dimensional oxovanadium−diphosphonate chains linked by Cu(II) square pyramids into two-dimensional layers. In contrast, compound **3** exhibits a two-dimensional oxovanadium−organodiphosphonate network, with Cu(II) sites decorating the surfaces. Compound **4** is unique in exhibiting a framework structure, which may be described as a three-dimensional oxovanadium−organodiphosphonate substructure with $\{Cu(phen)\}^{2+}$ subunits covalently attached to the surface of channels running parallel to the *a*-axis. The magnetic properties of **1**−**4** are also correlated to the structural characteristics. The magnetic behavior of **2** is thus dominated by antiferromagnetic interactions. The magnetic behavior of **1** and **4** is consistent with the presence of two distinct paramagnetic metal ions, Cu(II) and V(IV). In contrast, **3** does not exhibit ferrimagnetic behavior, but rather weak antiferromagnetic coupling. Crystal data: **1**, $C_{13}H_{10}N_2CuP_2VO_8$, monoclinic $P2_1/c$, $a = 9.0656(5)$ Å, $b = 8.6584(5)$ Å, $c = 20.934(1)$ Å, $\beta = 97.306(1)°$, $Z = 4$; **2**, $C_{26}H_{20}N_4Cu_2P_2V_2O_{11}$, triclinic $P\bar{1}$, $a = 10.6096(5)$ Å, $b = 11.6951(5)$ Å, $c = 13.1796(6)$ Å, $\alpha = 71.369(1)°$, $\beta = 70.790(1)°$, $\gamma = 80.738(1)°$, $Z = 2$; **3**, $C_{30}H_{28}N_4Cu_2P_4V_3O_{18}$, triclinic $P\bar{1}$, $a = 9.4356(6)$ Å, $b = 10.6556(6)$ Å, $c = 11.0354(7)$ Å, $\alpha = 118.187(1)°$, $\beta = 91.416(1)°$, $\gamma = 107.821(1)°$, $Z = 1$; **4**, $C_{26}H_{20}N_4Cu_2P_4V_3O_{18}$, monoclinic, $P2_1/c$ $a = 8.3947(3)$ Å, $b = 16.8401(7)$ Å, $c = 11.9144(5)$ Å, $\beta = 93.903(1)°$, $Z = 2$.

The oxovanadium phosphate (V−P−O) system represents an important subclass of the family of inorganic oxides. The dramatic expansion of the chemistry of the V−P−O system derives its impetus from the observation that vanadyl pyrophosphate $(VO)_2P_2O_7$[1,2] and vandyl phosphite[3,4] are effective in the selective air oxidation of butane to maleic anhydride, a remarkable transformation involving 14 electrons and seven oxygen atoms. In addition to studies directed at the elucidation of the catalytic reaction mechanism, the synthesis and characterization of related materials has provided an expansive chemical literature. The compositional range and structural diversity associated with the V−P−O phases reflects in part the versatility of vanadium oxide chemistry. Under the synthetic conditions exploited for the preparation of these phases, the V(III), V(IV), and V(V) oxidation states are readily accessible. Consequently, different vanadium coordination polyhedra, including tetrahedral [V(V)], square pyramidal [V(IV) and V(V)], trigonal bipyramidal [V(IV)], distorted octahedral [V(IV) and V(V)], and regular octahedral [V(III)] are available as structural building blocks. In addition, vanadium polyhedra may fuse through condensation via shared oxo groups into larger oxide aggregates $\{V_xO_y\}$ or even one-dimensional chains. The vanadium and phosphorus polyhedra may exhibit variable connectivities, sharing common corners, edges or faces and combinations of these modes. Water molecules and hydroxyl group participation in the vanadium ligation provide additional complexity.

Further structural elaboration of an inorganic oxide substructure may be achieved by introducing organic components, a powerful method for the synthesis of novel solid-state materials combining the unique characteristics of the inorganic and organic subunits in the design of composite materials.[5] It has

[†] Syracuse University.
[‡] McMaster University.

(1) Centi, G.; Trifiro, F.; Ebner, J. R.; Franchetti, V. M. *Chem. Rev.* **1988**, *88*, 55.
(2) Centi, G., Ed. Vanadyl Pyrophosphate Catalysts. *Catalysis Today*; Elsevier: Amsterdam, 1993; Vol. 16.
(3) Sananes, M. T.; Hutchings, G. J.; Volta, J.-C. *J. Chem. Soc., Chem. Commun.* **1995**, 243.
(4) Sananes, M. T.; Hutchings, G. J.; Volta, J.-C. *J. Catal.* **1995**, *154*, 253.
(5) Stupp, S. I.; Braun, P. V. *Science* **1997**, *277*, 1242.

10.1021/ic010186i CCC: $20.00
Published on Web 06/09/2001

been amply demonstrated in the chemistry of zeolites[6−8] that novel structures may be derived from the use of organocations as guests in the crystallizing product. The organic component effectively stabilizes the "void" regions within the inorganic structure by adopting charge compensating and space-filling roles,[9] with such guest species often referred to as templates or structure-directing agents.[10] The successful exploitation of organic cations as structure-directing components of zeolitic structures suggested that similar roles may be adopted in the design of open-framework materials based on transition metal-oxide polyhedra and appropriate negatively charged subunits, in place of aluminum and silicon tetrahedra. This expectation has been realized in the family of hybrid materials constructed from oxovanadium phosphate and organic cation subunits,[11−27] displaying structures ranging from simple one-dimensional chains in $(CN_3H_6)[(VO)(HPO_4)(H_2PO_4)(H_2O)]$ to complex three-dimensional microporous frameworks in $[HN(CH_2CH_2)_3NH]K_{1.35}[V_5O_9(PO_4)_2]$.

While organic structure-directing subunits are most commonly introduced as cationic components as noted, the evolution of inorganic phosphate materials has exploited direct derivatization of the tetrahedral phosphate subunit as a method for incorporating the organic moiety. Consequently, metal organophosphonates are prototypical composite materials, in which variations in the steric demands of the organic subunit, the tether length, and/or the presence of additional functional groups may be exploited to effect structural modifications.[28]

Oxovanadium−organophosphonate chemistry includes solid materials with one-, two-, and three-dimensional structures, incorporating either single valence V(IV) or V(V) sites or mixed-valence V(IV)/V(V) sites,[29−45] as well as molecular species exhibiting a remarkable structural diversity.[32] Furthermore, the structural chemistry of the oxovanadium−organophosphonate phases can be influenced not only by the length of the organic spacer but also by the introduction of organic cations as charge-compensating and space-filling entities with multipoint hydrogen-bonding interactions to the oxide backbone.

In the course of developing the chemistry of hybrid materials of the oxovanadium−organophosphonate family, the chemistry of the cationic component was elaborated by replacing the simple organic charge-compensating group with a transition-metal coordination complex cation,[46] so as to exploit the coordination preferences of this secondary metal site and the geometric variability attainable at the associated ligand center. In this way, both the spatial transmission of structural information by a diphosphonate ligand and the surface modification of the V−P−O substructure could be effected. Furthermore, the building block approach to new families of solid-state compounds has produced significant progress in the specific case of magnetochemistry,[47,48] as well as in "crystal engineering" and porous materials.[12,49,50] The strategy has led to many advances in the study of low-dimensional magnetic phenomena as a result of the relative ease in tuning the systems through the use of different spacers, ligands and metal complexes.[51−63] Since the oxovanadium-organophosphonate system represents

(6) Smith, J. V. *Chem. Rev.* **1988**, *88*, 149.
(7) Occelli, M. L.; Robson, H. C. *Zeolite Synthesis;* American Chemical Society: Washington, DC, 1989.
(8) Barrer, R. M. *Hydrothermal Chemistry of Zeolites*; Academic Press: New York, 1982.
(9) Wagner, P.; Nakagawa, Y.; Lee, G. S.; Davis, M. E.; Elomari, S.; Medrud, R. C.; Zones, S. I. *J. Am. Chem. Soc.* **2000**, *122*, 263.
(10) Lolio, R. F.; Zones, S. I.; Davis, M. G. In *Inclusion Chemistry with Zeolites, Nanoscale Materials by Design*; Herron, N., Corlim, D., Eds.; Kluwer Academic Press: Dordrecht, The Netherlands, 1995; Vol. 21, p 47.
(11) Soghomonian, V.; Chen, Q.; Haushalter, R. C., Zubieta, J.; O'Connor, C. J. *Science* **1993**, *259*, 1596.
(12) Khan, M. I.; Meyer, L. M.; Haushalter, R. C.; Schweitzer, A. L.; Zubieta, J.; Dye, J. L. *Chem. Mater.* **1996**, *8*, 43.
(13) Khan, M. I.; Haushalter, R. C.; O'Connor, C. J.; Tao, C.; Zubieta, J. *Chem. Mater.* **1995**, *7*, 593.
(14) Bircsak, Z.; Hall, A. K.; Harrison, W. T. A. *J. Solid State Chem.* **1999**, *142*, 168.
(15) Chippindale, A. M. *Chem. Mater.* **2000**, *12*, 818.
(16) (a) Soghomonian, V.; Haushalter, R. C.; Chen, Q.; Zubieta, J. *Inorg. Chem.* **1994**, *33*, 1700. (b) Riou, D.; Ferey, G. *Eur. J. Solid State Inorg. Chem.* **1994**, *31*, 25.
(17) Lu, Y.; Haushalter, R. C.; Zubieta, J. *Inorg. Chim. Acta* **1997**, *257*, 268.
(18) Bircsak, Z.; Harrison, W. T. A., *Inorg. Chem.* **1998**, *37*, 3204.
(19) Soghomonain, V.; Chen, Q.; Zhang, Y.; Haushalter, R. C.; O'Connor, C. J.; Tao, C.; Zubieta, J. *Inorg. Chem.* **1995**, *34*, 3509.
(20) Soghomonian, V.; Chen, Q.; Haushalter, R. C.; Zubieta, J.; O'Connor, C. J.; Lee, Y.-S. *Chem. Mater.* **1993**, *5*, 1690.
(21) Loiseau, T.; Férey, G. *J. Solid State Chem.* **1994**, *111*, 416.
(22) Soghomonian, V.; Chen, Q.; Haushalter, R. C.; Zubieta, J. *Chem. Mater.* **1993**, *5*, 1595.
(23) Soghomonian, V.; Haushalter, R. C.; Zubieta, J.; O'Connor, C. J. *Inorg. Chem.* **1996**, *35*, 2826.
(24) Bu, X.; Feng, P.; Stucky, G. D. *Chem. Commun.* **1995**, 1337.
(25) Soghomonian, V.; Chen, Q.; Haushalter, R. C.; Zubieta, J. *Angew. Chem., Int. Ed. Engl.* **1993**, *32*, 610.
(26) Harrison, W. T. A.; Hsu, K.; Jacobson, A. J. *Chem. Mater.* **1995**, *7*, 2004.
(27) Zhang, Y.; Clearfield, A.; Haushalter, R. C. *Chem. Mater.* **1995**, *7*, 1221.
(28) Clearfield, A. *Prog. Inorg. Chem.* **1998**, *47*, 371.
(29) Huan, G.; Jacobson, A. J.; Johnson, J. W.; Corcoran, E. W., Jr. *Chem. Mater.* **1990**, *2*, 91.
(30) Huan, G.; Johnson, J. W.; Jacobson, A. J.; Merola, J. S. *J. Solid State Chem.* **1990**, *89*, 220.
(31) Harrison, W. T. A.; Dussack, L. L.; Jacobson, A. J. *Inorg. Chem.* **1996**, *35*, 1461.
(32) Khan, M. I.; Zubieta, J. *Prog. Inorg. Chem.* **1995**, *43*, 1.
(33) Khan, M. I., Lee, Y.-S.; O'Connor, C. J.; Haushalter, R. S.; Zubieta, J. *Inorg. Chem.* **1994**, *33*, 3855.
(34) Khan, M. I.; Lee, Y.-S.; O'Connor, C. J.; Haushalter, R. S.; Zubieta, J. *Chem. Mater.* **1994**, *6*, 4525.
(35) Khan, M. I.; Lee, Y.-S.; O'Connor, C. J.; Haushalter, R. S.; Zubieta, J. *Chem. Mater.* **1994**, *6*, 721.
(36) Soghomonian, V.; Chen, Q.; Haushalter, R. C.; Zubieta, J. *Angew. Chem., Int. Ed. Engl.* **1995**, *34*, 4460.
(37) Soghomonian, V.; Diaz, R.; Haushalter, R. C.; O'Connor, C. J.; Zubieta, J. *Inorg. Chem.* **1995**, *34*, 4460.
(38) Soghomonian, V.; Haushalter, R. C.; Zubieta, J. *Chem. Mater.* **1995**, *7*, 1648.
(39) Bonavia, G.; Haushalter, R. C.; O'Connor, C. J.; Zubieta, J. *Inorg. Chem.* **1996**, *35*, 5603.
(40) Ninclaus, C.; Serre, C.; Riou, D.; Férey, G. *C. R. Acad. Sci. Paris Ser. IIc* **1998**, *1*, 551.
(41) Bonavia, G.; Haushalter, R. C.; Lu, S.; O'Connor, R. C.; Zubieta, J. *J. Solid State Chem.* **1997**, *132*, 144.
(42) Riou, D.; Serre, C.; Férey, G. *J. Solid State Chem.* **1998**, *141*, 89.
(43) Riou, D.; Roubeau, O.; Férey, G. *Microporous Mesoporous Mater.* **1998**, *23*, 23.
(44) Riou, D.; Férey, G. *J. Mater. Chem.* **1998**, *8*, 2733.
(45) Riou-Cavellec, M.; Sanselme, M.; Férey, G. *J. Mater. Chem.* **2000**, *10*, 745.
(46) Finn, R. C.; Zubieta, J. *J. Chem. Soc., Dalton Trans.* **2000**, 1821.
(47) *Reasearch Frontiers in Magnetochemistry*; O'Connor, C. J., Ed.; World Scientific Publishing Co.: Singapore, 1993.
(48) *Magnetic Molecular Materials;* Gatteschi, D., Kahn, O., Miller, J. S., Palacio, F., Eds.; Kluwer Academic Publishers: Dordrecht, 1991.
(49) Zawarotko, M. J., *Chem. Commun.* **2001**, 1.
(50) (a) Cheetham, A. K.; Férey, G.; Loiseau, T., *Angew. Chem., Int. Ed. Engl.* **1999**, *38*, 3268. (b) Férey, G., *C. R. Acad. Sci. Paris, Ser. IIc* **1998**, *1*, 1.
(51) Felthouse, T. R.; Hendrickson, D. N. *Inorg. Chem.* **1978**, *17*, 2636.
(52) Gleizes, A.; Verdaguer, M. *J. Am. Chem. Soc.* **1984**, *106*, 3727.
(53) Pei, Y.; Kahn, O.; Sletten, J.; Renard, J.-P.; Georges, R.; Gianduzzo, J.-C.; Curely, J.; Xu, Q. *Inorg. Chem.* **1988**, *27*, 47.
(54) Drillon, M.; Coronado, E.; Belaiche, M.; Carlin, R. L. *J. Appl. Phys.* **1988**, *63*, 3551.
(55) Nakatani, K.; Kahn, O.; Mathonière, C.; Pei, Y.; Zakine, C. *New J. Chem.* **1990**, *14*, 861.
(56) Sapiña, F.; Escrivá, E.; Folgado, J. V.; Beltrán, A.; Fuertes, A.; Drillon, M. *Inorg. Chem.* **1992**, *31*, 3851.

a rich class of organic/inorganic hybrid materials[64−66] whose structures can be influenced by the presence of organic spacers as well as incorporation of charge-compensating cations that can be of either organic or inorganic character, the structural diversity of these compounds, spanning one, two, and three dimensions, coupled with the presence of paramagnetic metal ions, make them ideal candidates for magnetic property studies. We have previously reported the isolation of a series of two-dimensional V−P−O networks, surface-modified by the presence of copper(II)−2,2′-bipyridine subunits, represented by [{Cu(2,2′-bpy)(H$_2$O)}(VO)(O$_3$PCH$_2$PO$_3$)], [Cu(2,2′-bpy)(VO)-(O$_3$PCH$_2$CH$_2$PO$_3$)], and [Cu(2,2′-bpy)(VO)(O$_3$PCH$_2$CH$_2$CH$_2$-PO$_3$)]·H$_2$O.[46] As part of these studies, the 2,2′-bpy component was replaced by 1,10-phenanthroline (phen) to investigate the consequence of the increased steric demand of the ligand. Hydrothermal synthesis provided four novel hybrid materials: the two-dimensional phases [Cu(phen)(VO)(O$_3$PCH$_2$PO$_3$)(H$_2$O)] (**1**), [{Cu(phen)}$_2$(V$_2$O$_5$)(O$_3$PCH$_2$CH$_2$PO$_3$)] (**2**), and [{Cu-(phen)}$_2$(V$_3$O$_5$)(O$_3$PCH$_2$CH$_2$ CH$_2$PO$_3$)$_2$(H$_2$O)] (**3**) and the three-dimensional [{Cu(phen)}$_2$(V$_3$O$_5$)(O$_3$PCH$_2$PO$_3$)$_2$(H$_2$O)] (**4**), whose structures and magnetic properties are presented.

Experimental Section

Reagents were purchased from Aldrich Chemical Co. and used without further purification. All syntheses were carried out in 23 mL poly(tetrafluoroethylene)-lined stainless steel containers under autogenous pressure. The reactants were stirred briefly before heating. Water was distilled above 3.0 Ω in-house using a Barnstead Model 525 Biopure distilled water center.

Synthesis of [Cu(phen)(VO)(O$_3$PCH$_2$PO$_3$)(H$_2$O)] (1). A mixture of CuCl$_2$·2H$_2$O (0.089 g, 0.52 mmol), methylenediphosphonic acid (0.065 g, 0.36 mmol), Na$_3$VO$_4$ (0.060 g, 0.33 mmol), 1,10-phenanthroline (0.061 g, 0.34 mmol), 40% (*n*-C$_4$H$_9$)$_4$NOH (0.163 g, 0.63 mmol), and H$_2$O,(10.16 g, 564 mmol) in the mole ratio 1.6:1.1:1.0:1.0:4.9:1700 was heated for 46 h at 200 °C. After the mixture was cooled to room temperature, green crystals of **1** were isolated in 30% yield. IR (KBr pellet, cm^{-1}): 1516 (m), 1426 (s), 1167 (s), 1121 (s), 1068 (s), 1036 (s), 993 (s), 846 (m), 769 (m), 722 (m), 648 (m).

Synthesis of [{Cu(phen)}$_2$(V$_2$O$_5$)(O$_3$PCH$_2$CH$_2$PO$_3$)] (2). A mixture of CuCl$_2$·2H$_2$O (0.098 g, 0.58 mmol), ethylene diphosphonic acid (0.109 g, 0.58 mmol), Na$_3$VO$_4$ (0.103 g, 0.56 mmol), 1,10-phenanthroline (0.104 g, 0.57 mmol), and H$_2$O (15.7 g, 870 mmol) in the mole ratio 1.0:1.0:1.0:1.0:1500 was heated for 42 h at 180 °C. Green crystals of **2** were recovered in 40% yield: IR (KBr pellet, cm^{-1}) 1427 (m), 1177 (s), 1163 (s), 1050 (s), 953 (s), 906 (s), 859 (s), 790 (s), 721 (m), 649 (m).

Synthesis of [{Cu(phen)}$_2$(V$_3$O$_5$)(O$_3$PCH$_2$CH$_2$CH$_2$PO$_3$)$_2$(H$_2$O)] (3). A mixture of CuCl$_2$·H$_2$O (0.097 g, 0.57 mmol), 1,3-propylene diphosphonic acid (0.059 g, 0.29 mmol), Na$_3$VO$_4$ (0.101 g, 0.57 mmol), 1,10-phenanthroline (0.078 g, 0.43 mmol), and H$_2$O (10.24 g, 569 mmol) in the mole ratio 2.0:1.0:2.0:1.5:2000 was heated at 180 °C for 40 h. After the mixture was cooled to room temperature, dark green crystals of **3** were recovered in ca. 35−40% yield: IR (KBr pellet, cm^{-1}) 1426 (m), 1144 (s), 1107 (s), 1021 (s), 972 (s), 922 (m), 856 (m), 721 (m).

Synthesis of [{Cu(phen)}$_2$(V$_3$O$_5$)(O$_3$PCH$_2$PO$_3$)$_2$(H$_2$O)] (4). A mixture of CuCl$_2$·2H$_2$O (0.102 g, 0.60 mmol), methylenediphosphonic acid (0.064 g, 0.36 mmol), Na$_3$VO$_4$ (0.046 g, 0.25 mmol), 1,10-phenanthroline (0.051 g, 0.28 mmol), and H$_2$O (10.04 g, 556 mmol) in the mole ratio 2.4:1.4:1.0:1.1:2200 was heated at 180 °C for 41 h. Blue crystals of **4** were recovered in 60% yield: IR (KBr pellet, cm^{-1}) 1521 (m), 1429 (m), 1142 (s), 1085 (s), 978 (s), 941 (s), 855 (m), 769 (s), 722 (m).

X-ray Crystallography. Structural measurements for **1**−**4** were performed on a Bruker SMART-CCD[67] diffractometer at a temperature of 100 ± 1 K using graphite-monochromated Mo Kα radiation (λ(Mo Kα) = 0.71073 Å). The data were corrected for Lorentz and polarization effects and absorption using SADABS.[68] The structures were solved by direct methods.[69] All of the non-hydrogen atoms were located from the initial solution or from subsequent electron density difference maps during the initial stages of the refinement. After all of the non-hydrogen atoms in each structure were located, the models were refined against F^2, first using isotropic and finally anisotropic thermal displacement parameters, until the final value of σ/Δ_{max} was less than 0.001. The positions of the hydrogen atoms were then calculated and fixed, and a final cycle of refinements was performed until σ/Δ_{max} was less than 0.001. Neutral atom scattering coefficients and anomalous dispersion corrections were taken from the *International Tables for X-ray Crystallography*, Vol. C.[70] All calculations were performed using the SHELXTL[69] crystallographic software packages.

In the case of compound **3**, the V(1) and O2 sites are disordered about the inversion center, so as to produce equal populations of the two alignments of the {V═O} vector with respect to the basal plane. Likewise, the V(2) site is disordered along the V(2)−O(6) vector with relative occupancies of 0.9 and 0.1 for the two orientations.

The V(1) site of compound **4** is also disordered about the inversion center at 1/2 1/2 1/2. This results in a statistical disordering of the vanadium along the {O = V−OH$_2$} vector so as to alternate the V═O unit between the two orientations along the vector.

Crystallographic details for the structures of **1**−**4** are summarized in Table 1. Atomic positional parameters, full tables of bond lengths and angles and anisotropic temperature factors are available in the Supporting Information. Selected bond lengths and angles for **1**−**4** are given in Tables 2−5, respectively.

Magnetic Measurements. Samples (30−100 mg) were placed in gel-cap holders and accurately weighed prior to data collection. Zero-field-cooled (ZFC) and field-cooled (FC) magnetic susceptibility data were collected on a Quantum Design Squid magnetometer between 2 and 350 K with an applied field of 500 Oe. For clarity, only the ZFC data are shown in the figures since no divergence was observed for all samples. Diamagnetic corrections were applied to the data using Pascal's constants in emu mol^{-1} units (-2.7×10^{-4} (**1**), -4.5×10^{-4} (**2**), -6.0×10^{-4} (**3**), -5.6 X 10^{-4} (**4**)).[71]

Results and Discussion

Syntheses, Infrared Spectroscopy, and Structures. The isolation of compounds **1**−**4** relies on hydrothermal techniques,[72−74] which have now witnessed extensive application

(57) DeBord, J. R. D.; Zhang, Y.; Haushalter, R. C.; Zubieta, J.; O'Connor, C. J. *J. Solid State Chem.* **1996**, *122*, 251.
(58) Rabu, P.; Rouba, S.; Laget, V.; Hornick, C.; Drillon, M. *Chem. Commun.* **1996**, 1107.
(59) Cador, O.; Price, D.; Larionova, J.; Mathonière, C.; Kahn, O.; Yakhmi, J. V. *J. Mater. Chem.* **1997**, *7*, 1263.
(60) Surville-Barland, C.; Ruiz, R.; Aukauloo, A.; Journaux. Y.; Castro, I.; Cervera, B.; Julve, M.; LLoret, F.; Sapiña, F. *Inorg. Chim. Acta* **1998**, *278*, 159.
(61) Breeze, S. R.; Wang, S.; Greedan, J. E.; Raju, N. P. *J. Chem. Soc., Dalton Trans.* **1998**, 2327.
(62) Rittenberg, D. K.; Miller, J. S. *Inorg. Chem.* **1999**, *38*, 4838.
(63) Carcia, Y.; Koningsbruggen, P. J. van; Kooijman, H.; Spek, A. L.; Haasnoot, J. G.; Kahn, O. *Eur. J. Inorg. Chem.* **2000**, 307.
(64) Drillon, M.; Panissod, P. *J. Magn. Magn. Mater.* **1998**, *188*, 93.
(65) Williams, I. D.; Law, T. S.-C.; Sung, H. H.-Y.; Wen, G.-H.; Zhang, X.-X. *Solid State Sci.* **2000**, *2*, 47.
(66) Hornick, C.; Rabu, P.; Drillon, M. *Polyhedron* **2000**, *19*, 259.
(67) Siemens *SMART Software Reference Manual*; Siemens Analytical X-ray Instruments, Inc.: Madison, WI, 1994.
(68) Sheldrick, G. M. *SADABS: Program for Empirical Absorption Corrections*; Sheldrick, G. M., Ed.; University of Gottingen: Germany, 1996.
(69) Sheldrick, G. M. *SHELXL96. Program for the Refinement of Crystal Structures*; Sheldrick, G. M., Ed.; University of Gottingen, Germany, 1996.
(70) *International Tables for X-ray Crystallography*; Vol. C, Tables 4.2.6.8 and 6.1.1.4; Kluwer Academic: Boston, 1992.
(71) *Theory and Applications of Molecular Diamagnetism;* Mulay, L. N., Boudreaux, E. A., Eds.; Wiley-Interscience Publication: New York, 1976.
(72) Rabenau, A. *Angew. Chem., Int. Ed. Engl.* **1985**, *24*, 1026.
(73) Laudise, R. A. *Chem. Eng. News* **1987**, Sept. 28, 30.
(74) Gopalakrishnan, J. *Chem. Mater.* **1995**, *7*, 1265.

Table 1. Summary of Crystal Data for [Cu(phen)(VO)($O_3PCH_2PO_3$)(H_2O)] (**1**), [{Cu(phen)}$_2$(V_2O_5)($O_3PCH_2CH_2PO_3$)] (**2**), [{Cu(phen)}$_2$(V_3O_5)($O_3PCH_2CH_2CH_2PO_3$)$_2$(H_2O)] (**3**), and [{Cu(phen)}$_2$(V_3O_5)($O_3PCH_2PO_3$)$_2$(H_2O)] (**4**)

	1	**2**	**3**	**4**
emp formula	$C_{13}H_{10}N_2CuP_2VO_8$	$C_{26}H_{20}N_4Cu_2P_2V_2O_{11}$	$C_{30}H_{28}N_4Cu_2P_4V_3O_{18}$	$C_{26}H_{20}N_4Cu_2P_4V_3O_{18}$
fw	498.65	855.36	1136.34	1080.24
space group	$P2_1/c$	$P\bar{1}$	$P\bar{1}$	$P2_1/c$
a, Å	9.0656(5)	10.6096(5)	9.4356(6)	8.3947(3)
b, Å	8.6584(5)	11.6951(5)	10.6556(6)	16.8401(7)
c, Å	20.934(1)	13.1796(6)	11.0354(7)	11.9144(5)
α, deg	90.0	71.369(1)	118.187(1)	90.0
β, deg	97.306(1)	70.790(1)	91.416(1)	93.903(1)
γ, deg	90.0	80.738(1)	107.821(1)	90.6
V, Å^3	1629.8(2)	1460.5(1)	911.8(1)	1680.4(2)
Z	4	2	1	2
D_{calc}, gcm^{-3}	2.032	1.945	2.069	2.135
μ, cm^{-1}	21.24	22.36	21.52	23.30
λ, Mo Kα	0.71073	0.71073	0.71073	0.71073
R1a	0.0399	0.0400	0.0396	0.0318
wR2b	0.0994	0.1088	0.1107	0.0805

[a] $\Sigma||Fo| - |Fc||/|Fo|$. [b] $\Sigma[w(Fo^2 - Fc^2)^2]/\Sigma[w(Fo^2)^2]]^{1/2}$.

Table 2. Selected Bond Lengths (Å) and Angles (Deg) for [Cu(phen)(VO)($O_3PCH_2PO_3$)(H_2O)] (**1**)

Cu(1)−O(1)	1.932(2)	O(1)−Cu(1)−O(3)	95.85(10)	O(3)−P(1)−O(7)	111.96(15)
Cu(1)−O(3)	1.947(2)	O(1)−Cu(1)−N(1)	89.39(11)	O(3)−P(1)−O(4)	110.23(14)
Cu(1)−N(1)	2.020(3)	O(3)−Cu(1)−N(1)	166.08(12)	O(7)−P(1)−O(4)	109.77(14)
Cu(1)−N(2)	2.038(3)	O(1)−Cu(1)−N(2)	159.83(11)	O(3)−P(1)−C(13)	109.55(15)
Cu(1)−O(2)	2.180(2)	O(3)−Cu(1)−N(2)	89.63(11)	O(7)−P(1)−C(13)	106.98(15)
V(1)−O(8)	1.604(3)	N(1)−Cu(1)−N(2)	81.27(12)	O(4)−P(1)−C(13)	108.23(16)
V(1)−O(6)	1.944(2)	O(1)−Cu(1)−O(2)	104.94(10)	O(2)−P(2)−O(1)	111.09(14)
V(1)−O(4)	1.949(3)	O(3)−Cu(1)−O(2)	91.27(10)	O(2)−P(2)−O(6)	110.91(14)
V(1)−O(7)	1.967(2)	N(1)−Cu(1)−O(2)	99.85(11)	O(1)−P(2)−O(6)	112.43(15)
V(1)−O(5)	2.033(3)	N(2)−Cu(1)−O(2)	94.29(11)	O(2)−P(2)−C(13)	110.53(16)
P(1)−O(3)	1.519(3)			O(1)−P(2)−C(13)	106.54(15)
P(1)−O(7)	1.530(3)	O(8)−V(1)−O(6)	112.82(13)	O(6)−P(2)−C(13)	105.08(15)
P(1)−O(4)	1.533(2)	O(8)−V(1)−O(4)	112.30(12)		
P(1)−C(13)	1.805(4)	O(6)−V(1)−O(4)	134.88(12)	P(2)−O(1)−Cu(1)	130.50(14)
P(2)−O(2)	1.518(2)	O(8)−V(1)−O(7)	100.88(13)	P(2)−O(2)−Cu(1)	134.38(14)
P(2)−O(1)	1.526(3)	O(6)−V(1)−O(7)	90.52(10)	P(1)−O(3)−Cu(1)	128.11(15)
P(2)−O(6)	1.550(3)	O(4)−V(1)−O(7)	80.64(10)	P(1)−O(4)−V(1)	145.18(16)
P(2)−C(13)	1.816(3)	O(8)−V(1)−O(5)	100.03(12)	P(2)−O(6)−V(1)	139.31(15)
		O(6)−V(1)−O(5)	84.70(10)	P(1)−O(7)−V(1)	135.62(15)
		O(4)−V(1)−O(5)	88.13(10)		
		O(7)−V(1)−O(5)	158.77(11)		

not only in the synthesis of zeolites[8] but also in the isolation of molybdenum oxides,[75−78] metal halides and pseudohalides,[79,80] and metal phosphates and phosphonates.[81,11−46] Hydrothermal synthesis exploits the reduced viscosity of water at temperatures above 100 °C and autogenous pressure to promote solvent extraction of solids and crystal growth from solution. Another advantage of the method for the preparation of hybrid materials is the ready solubilization of both organic and inorganic starting materials which alleviates differential solubility problems. The working temperature range of 120−250 °C, in contrast to the elevated temperatures of conventional solid-state syntheses, allows retention of the structural integrity of the organic constituents and promotes "self-assembly" of metastable phases from simple molecular precursors.

The syntheses of compounds **1**−**4** were effected through straightforward application of these principles. In general, hydrothermal reactions of $CuCl_2{\cdot}2H_2O$, Na_3VO_4, 1,10-phenanthroline and the appropriate diphosphonate of 40−46 h duration at temperatures of 180−200 °C produced the compounds as monophasic materials in 30−60% yield. In the case of compound **1**, the pH of the starting solution was adjusted by the addition of (n-C_4H_9)NOH in the synthetic optimization.

The infrared spectra of compounds **1**−**4** exhibit in all cases a series of three or four strong bands in the 1000−1200 cm^{-1} range associated with ν(P−O) of the diphosphonate ligands. Characteristic phen features are observed between 1400 and 1550 cm^{-1}.

The infrared spectrum of [Cu(phen)(VO)($O_3PCH_2PO_3$)(H_2O)] (**1**) exhibits a strong absorption at 993 cm^{-1} attributed to ν(V═O) for V(IV) site. In contrast, the V(V) species [{Cu(phen)}$_2$-(V_2O_5)($O_3PCH_2CH_2PO_3$)] (**2**) exhibits strong bands at 953 and 906 cm^{-1}, attributed to ν(V═O) and ν(V═O···Cu). The lower frequency of these bands compared to that of **1** is consistent with the V(V) oxidation. The mixed valence compound [{Cu-(phen)}$_2$(V_3O_5)($O_3PCH_2CH_2CH_2PO_3$)$_2$(H_2O)] (**3**) exhibits a strong band at 972 cm^{-1} and a weaker feature at 922 cm^{-1} attributed to ν(V═O) for the V(IV) and V(V) sites, respectively. The three-dimensional material [{Cu(phen)}$_2$(V_3O_5)(O_3PCH_2-

(75) Hagrman, P. J.; Hagrman, D.; Zubieta, J. *Angew. Chem., Int. Ed. Engl.* **1999**, *38*, 2638.
(76) Chesnut, D. J.; Hagrman, D.; Zapf, P. J.; Hammond, R. P.; LaDuca, R.; Haushalter, R. C.; Zubieta, J. *Coord. Chem. Rev.* **1999**, *190*−*192*, 737.
(77) Hagrman, D.; Zubieta, J. *Trans. Am. Crystallogr. Assoc.* **1998**, *33*, 109.
(78) Hagrman, D.; Hagrman, P. J.; Zubieta, J. *Comments Inorg. Chem.* **1999**, *21*, 225.
(79) See, for example: (a) Francis, R. J.; Halasyamani, P. S.; O'Hare, D. *Angew. Chem., Int. Ed. Engl.* **1998**, *37*, 2214. (b) Mitzi, D. *Chem. Mater.* **1996**, *8*, 791. (c) DeBord, J. R. D.; Lu, Y.-J.; Warren, C. J.; Haushalter, R. C.; Zubieta, J. *Chem. Commun.* **1997**, 1365.
(80) (a) Chesnut, D. J.; Kusnetzow, A.; Zubieta, J. *J. Chem. Soc., Dalton Trans.* **1998**, 4081. (b) Chesnut, D. J.; Zubieta, J. *Chem. Commun.* **1998**, 1707. (c) Chesnut, D. J.; Kuznetzow, A.; Birge, R. R., Zubieta, J. *Inorg. Chem.* **1999**, *38*, 2663.

Table 3. Selected Bond Lengths (Å) and Angles (Deg) for $[\{Cu(phen)\}_2(V_2O_5)(O_3PCH_2CH_2PO_3)]$ (**2**)

Cu(1)−O(11)	1.933(2)	O(11)−Cu(1)−O(10)	96.58(8)	O(8)−V(2)−O(7)	108.80(12)
Cu(1)−O(10)	1.938(2)	O(11)−Cu(1)−N(3)	88.90(9)	O(8)−V(2)−O(6)	109.71(10)
Cu(1)−N(3)	2.012(2)	O(10)−Cu(1)−N(3)	169.69(9)	O(7)−V(2)−O(6)	112.48(10)
Cu(1)−N(4)	2.031(2)	O(11)−Cu(1)−N(4)	159.81(9)	O(8)−V(2)−O(9)	108.15(10)
Cu(1)−O(7)	2.258(2)	O(10)−Cu(1)−N(4)	90.89(9)	O(7)−V(2)−O(9)	104.52(10)
Cu(2)−O(1)	1.924(2)	N(3)−Cu(1)−N(4)	81.17(10)	O(6)−V(2)−O(9)	112.95(9)
Cu(2)−O(3)	1.925(2)	O(11)−Cu(1)−O(7)	101.32(8)		
Cu(2)−N(1)	2.006(2)	O(10)−Cu(1)−O(7)	96.24(8)	O(11)−P(1)−O(10)	115.97(12)
Cu(2)−N(2)	2.029(2)	N(3)−Cu(1)−O(7)	91.20(8)	O(11)−P(1)−O(9)	110.28(11)
Cu(2)−O(2)	2.344(2)	N(4)−Cu(1)−O(7)	96.45(9)	O(10)−P(1)−O(9)	110.41(11)
V(1)−O(5)	1.616(2)	O(1)−Cu(2)−O(3)	95.38(8)	O(11)−P(1)−C(25)	106.75(12)
V(1)−O(2)	1.647(2)	O(1)−Cu(2)−N(1)	167.57(9)	O(10)−P(1)−C(25)	108.51(12)
V(1)−O(6)	1.805(2)	O(3)−Cu(2)−N(1)	89.02(9)	O(9)−P(1)−C(25)	104.17(12)
V(1)−O(4)	1.871(2)	O(1)−Cu(2)−N(2)	92.21(9)	O(1)−P(2)−O(3)	114.66(11)
V(2)−O(8)	1.620(2)	O(3)−Cu(2)−N(2)	167.10(9)	O(1)−P(2)−O(4)	111.60(11)
V(2)−O(7)	1.642(2)	N(1)−Cu(2)−N(2)	81.50(10)	O(3)−P(2)−O(4)	110.01(11)
V(2)−O(6)	1.805(2)	O(1)−Cu(2)−O(2)	91.99(8)	O(1)−P(2)−C(26)	105.54(12)
V(2)−O(9)	1.875(2)	O(3)−Cu(2)−O(2)	105.69(8)	O(3)−P(2)−C(26)	107.73(12)
P(1)−O(11)	1.504(2)	N(1)−Cu(2)−O(2)	98.00(8)	O(4)−P(2)−C(26)	106.85(12)
P(1)−O(10)	1.517(2)	N(2)−Cu(2)−O(2)	84.41(8)		
P(1)−O(9)	1.570(2)			P(2)−O(1)−Cu(2)	133.16(12)
P(1)−C(25)	1.802(3)	O(5)−V(1)−O(2)	108.78(11)	V(1)−O(2)−Cu(2)	119.52(10)
P(2)−O(1)	1.515(2)	O(5)−V(1)−O(6)	111.23(10)	P(2)−O(3)−Cu(2)	132.26(12)
P(2)−O(3)	1.517(2)	O(2)−V(1)−O(6)	109.70(10)	P(2)−O(4)−V(1)	130.08(12)
P(2)−O(4)	1.564(2)	O(5)−V(1)−O(4)	107.80(10)	V(2)−O(6)−V(1)	136.37(12)
P(2)−C(26)	1.799(3)	O(2)−V(1)−O(4)	107.22(9)	V(2)−O(7)−Cu(1)	116.81(11)
		O(6)−V(1)−O(4)	111.99(9)		

Table 4. Selected Bond Lengths (Å) and Angles (Deg) for $[\{Cu(phen)\}_2(V_3O_5)(O_3PCH_2CH_2CH_2PO_3)_2(H_2O)]$ (**3**)

Cu(1)−O(4)	1.905(2)	O(4)−Cu(1)−O(1)	93.23(9)	O(4)−P(1)−O(3)	110.34(12)
Cu(1)−O(1)	1.922(2)	O(4)−Cu(1)−N(2)	92.51(9)	O(4)−P(1)−O(5)	115.85(12)
Cu(1)−N(2)	2.016(2)	O(1)−Cu(1)−N(2)	170.34(9)	O(3)−P(1)−O(5)	110.76(11)
Cu(1)−N(1)	2.020(3)	O(4)−Cu(1)−N(1)	170.89(9)	O(4)−P(1)−C(13)	106.34(13)
Cu(1)−O(2)	2.303(9)	O(1)−Cu(1)−N(1)	91.74(10)	O(3)−P(1)−C(13)	105.92(12)
V(1)−O(2)	1.608(7)	N(2)−Cu(1)−N(1)	81.58(10)	O(5)−P(1)−C(13)	107.01(13)
V(1)−O(8)	1.862(2)	O(4)−Cu(1)−O(2)	99.2(4)	O(1)−P(2)−O(7)	113.08(12)
V(1)−O(9)	1.903(2)	O(1)−Cu(1)−O(2)	97.47(17)	O(1)−P(2)−O(9)	110.30(12)
V(1)−O(8)#1	2.008(2)	N(2)−Cu(1)−O(2)	89.27(18)	O(7)−P(2)−O(9)	111.50(11)
V(1)−O(9)#1	2.017(2)	N(1)−Cu(1)−O(2)	87.7(4)	O(1)−P(2)−C(15)	107.69(12)
V(2)−O(6)	1.597(2)			O(7)−P(2)−C(15)	107.82(12)
V(2)−O(8)	1.734(2)	O(2)−V(1)−O(8)	106.2(5)	O(9)−P(2)−C(15)	106.10(12)
V(2)−O(3)	1.930(2)	O(2)−V(1)−O(9)	107.7(3)		
V(2)−O(7)	1.950(2)	O(8)−V(1)−O(9)	88.55(9)	P(2)−O(1)−Cu(1)	122.89(12)
V(2)−O(5)	1.968(2)	O(2) −V(1)−O(8)	104.9(5)	V(1)−O(2)−Cu(1)	126.4(5)
P(1)−O(4)	1.515(2)	O(2)−V(1)−O(9)	103.1(3)	P(1)−O(3)−V(2)	150.98(14)
P(1)−O(3)	1.532(2)	O(6)−V(2)−O(8)	105.63(11)	P(1)−O(4)−Cu(1)	144.29(14)
P(1)−O(5)	1.534(2)	O(6)−V(2)−O(3)	98.42(10)	P(1)−O(5)−V(2)	149.11(13)
P(1)−C(13)	1.794(3)	O(8)−V(2)−O(3)	92.46(9)	P(2)−O(7)−V(2)	133.28(12)
P(2)−O(1)	1.519(2)	O(6)−V(2)−O(7)	97.80(10)	V(2)−O(8)−V(1)	143.73(13)
P(2)−O(7)	1.530(2)	O(8)−V(2)−O(7)	89.57(9)	V(2)−O(8)−V(1)	115.90(12)
P(2)−O(9)	1.552(2)	O(3)−V(2)−O(7)	162.45(9)	P(2)−O(9)−V(1)	137.60(13)
P(2)−C(15)	1.795(3)	O(6)−V(2)−O(5)	108.88(10)		
		O(8)−V(2)−O(5)	145.37(10)		
		O(3)−V(2)−O(5)	85.44(8)		
		O(7)−V(2)−O(5)	83.02(8)		

$PO_3)_2(H_2O)]$ (**4**) likewise exhibits two strong absorptions at 978 and 941 cm^{-1}, consistent with $\nu(V{=}O)$ from V(IV) and V(V) sites, respectively.

As shown in Figure 1, the structure of $[Cu(phen)(VO)(O_3PCH_2PO_3)(H_2O)]$ consists of two-dimensional networks constructed from corner-sharing Cu(II) square-pyramids, V(IV) square pyramids, and phosphorus tetrahedra. The coordination sphere of the Cu(II) site is defined by the nitrogen donors of the phenanthroline ligand and two oxygen donors from a chelating methylenediphosphonate ligand in the basal plane, and by an oxygen donor from a second methylenediphosphonate group occupying the apical position. The basal plane of the V(IV) center consists of two oxygen donors from a chelating methylenediphosphonate ligand, an oxygen donor from a second methylenediphosphonate group and the aqua ligand; the apical position is occupied by the terminal oxo-group. Consequently, each methylenediphosphonate ligand bridges two V(IV) and two Cu(II) sites.

The network structure of **1** may be described in terms of undulating $\{(VO)(O_3PCH_2PO_3)\}_n^{2n-}$ chains linked by $\{CuO_3N_2\}$ sites into a two-dimensional structure. It is instructive to compare the structure of **1** to that of the analogous bipyridine compound $[Cu(2,2'\text{-bpy})(VO)(O_3PCH_2PO_3)(H_2O)]$. Although the compounds share a common formulation $[Cu(ligand)(VO)(O_3PCH_2PO_3)(H_2O)]$, the structural details are quite distinct. While the aqua ligand in **1** is bound to the V(IV) center, that of $[Cu(2,2'\text{-bpy})(VO)(O_3PCH_2PO_3)(H_2O)]$ is associated with the Cu(II) site. Consequently, as shown in Figure 2, the structure of the bipyridyl derivative may be described as a two-dimensional $\{(VO)(O_3PCH_2PO_3)\}_n^{2n-}$ network, decorated by

Table 5. Selected Bond Lengths (Å) and Angles (Deg) for [{Cu(phen)}$_2$(V_3O_5)($O_3PCH_2PO_3$)$_2$(H_2O)] (**4**)

Cu(1)−O(3)	1.931(2)	O(3)−Cu(1)−O(1)	96.11(7)	O(3)−P(1)−O(4)	115.02(11)
Cu(1)−O(1)	1.942(2)	O(3)−Cu(1)−N(2)	172.87(8)	O(3)−P(1)−O(8)	108.80(10)
Cu(1)−N(2)	2.002(2)	O(1)−Cu(1)−N(2)	89.37(8)	O(4)−P(1)−O(8)	108.54(10)
Cu(1)−N(1)	2.004(2)	O(3)−Cu(1)−N(1)	90.97(8)	O(3)−P(1)−C(13)	108.27(11)
Cu(1)−O(2)	2.357(2)	O(1)−Cu(1)−N(1)	160.60(8)	O(4)−P(1)−C(13)	107.07(11)
V(1)−O(9)	1.636(2)	N(2)−Cu(1)−N(1)	82.41(8)	O(8)−P(1)−C(13)	108.99(10)
V(1)−O(5)	1.992(2)	O(3)−Cu(1)−O(2)	91.18(7)	O(1)−P(2)−O(5)	114.85(11)
V(1)−O(4)	1.992(2)	O(1)−Cu(1)−O(2)	103.16(7)	O(1)−P(2)−O(6)	108.89(10)
V(1)−O(4)#1	2.011(2)	N(2)−Cu(1)−O(2)	92.00(7)	O(5)−P(2)−O(6)	108.34(10)
V(1)−O(5)	2.022(2)	N(1)−Cu(1)−O(2)	94.70(7)	O(1)−P(2)−C(13)	108.35(11)
V(1)−O(9)	2.314(2)			O(5)−P(2)−C(13)	107.22(11)
V(2)−O(7)	1.611(2)	O(9)−V(1)−O(5)	99.99(10)	O(6)−P(2)−C(13)	109.06(10)
V(2)−O(2)	1.635(2)	O(9)−V(1)−O(4)	99.45(10)		
V(2)−O(8)	1.855(2)	O(5)−V(1)−O(4)	90.08(8)	P(2)−O(1)−Cu(1)	130.35(11)
V(2)−O(6)	1.871(2)	O(9)−V(1)−O(5)	99.48(10)	V(2)−O(2)−Cu(1)	130.95(10)
P(1)−O(3)	1.512(2)	O(7)−V(2)−O(2)	108.68(9)	P(1)−O(3)−Cu(1)	130.61(11)
P(1)−O(4)	1.514(2)	O(7)−V(2)−O(8)	107.00(9)	P(1)−O(4)−V(1)	136.88(11)
P(1)−O(8)	1.555(2)	O(2)−V(2)−O(8)	109.22(8)	P(2)−O(5)−V(1)	130.00(11)
P(1)−C(13)	1.803(2)	O(7)−V(2)−O(6)	107.07(9)	P(2)−O(6)−V(2)	131.81(10)
P(2)−O(1)	1.512(2)	O(2)−V(2)−O(6)	110.57(8)	P(1)−O(8)−V(2)	145.25(12)
P(2)−O(5)	1.515(2)	O(8)−V(2)−O(6)	114.10(8)		
P(2)−O(6)	1.563(2)				
P(2)−C(13)	1.810(2)				

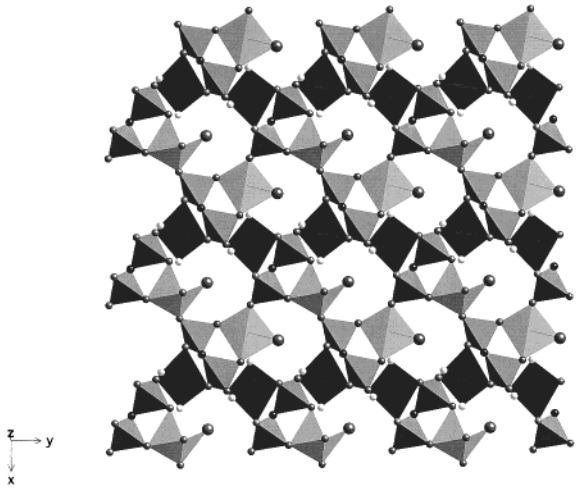

Figure 1. Polyhedral representation of the layer structure of [Cu(phen)-(VO)($O_3PCH_2PO_3$) (H_2O)] (**1**). The dark square pyramids are the Cu sites; the lighter square pyramids are V sites; the tetrahedra are P sites. Nitrogen atoms are shown as light spheres; oxygen atoms and the carbon of the diphosphonate are shown as dark spheres. The water oxygen atom bound to the vanadium is shown as a larger sphere to distinguish it from the oxo groups. The ligand carbon atoms have been omitted for clarity.

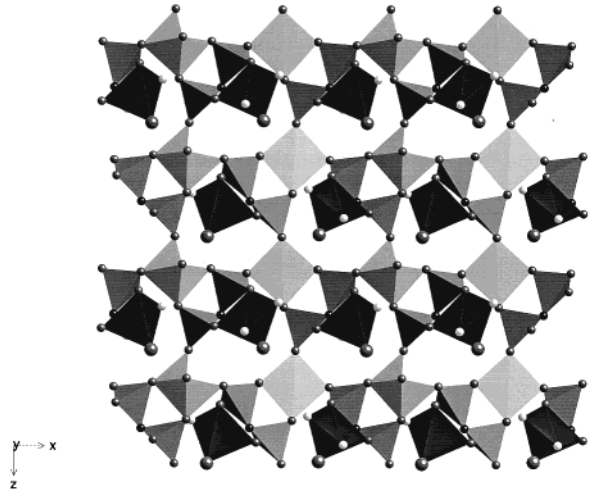

Figure 2. Polyhedral representation of the structure of [Cu(2,2′-bpy)-(VO)($O_3PCH_2PO_3$)(H_2O)]. The same conventions are used as those adopted for Figure 1.

$\{CuO_3N_2\}$ square pyramids which project into the interlamellar regions. While the Cu(II) site is an integral component of the network connectivity in **1**, the network structure of [Cu(2,2′-bpy)(VO)($O_3PCH_2PO_3$)(H_2O)] is established by the V−P−O−C substructure alone. Since the organoimine ligands in both **1** and [Cu(2,2′-bpy)(VO)($O_3PCH_2PO_3$)(H_2O)] project out of the oxide plane, it does not appear that steric arguments can be invoked for the dramatic structural changes. The factors controlling the location of the aqua ligand and consequently the network connectivity remain obscure.

The network structure of [{Cu(phen)}$_2$(V_2O_5)($O_3PCH_2CH_2$-PO_3)] (**2**), shown in Figure 3, is quite distinct from that adopted by **1**. In this case, the polyhedral connectivity of the layer involves corner-sharing of Cu(II) square pyramids, V(V) tetrahedra, and phosphorus tetrahedra linked through the ethylene chain. The Cu(II) site is considerably distorted from the idealized square pyramidal limit, with the geometry defined by two nitrogen donors from the phenanthroline ligand, two oxygen

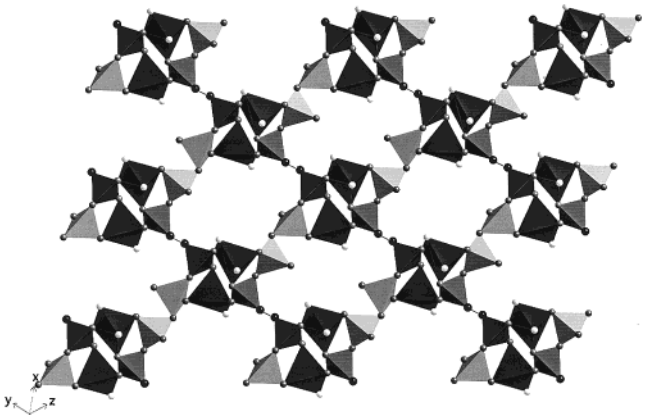

Figure 3. Polyhedral view of the network structure of [{Cu(phen)}$_2$-(V_2O_5)($O_3PCH_2CH_2PO_3$)] (**2**).

donors, one from each of two ethylenediphosphonate ligands and a bridging oxo-group to a V(V) site. The coordination spheres of the V(V) centers are defined by a terminal oxo-group, an oxo-group bridging to a V(V) center, an oxo-group bridging to the Cu(II) site, and an oxygen from an ethylenediphosphonate

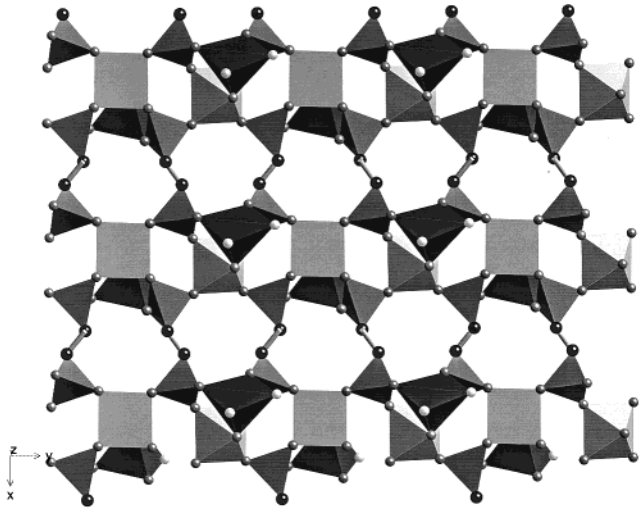

Figure 4. Polyhedral view of the network structure of [Cu(2,2′-bpy)(VO)($O_3PCH_2CH_2PO_3$)].

ligand. The corner-sharing interaction between vanadium tetrahedra results in a binuclear V(V) site $\{V_2O_7\}$; this unit in turn engages in oxo-bridging to two Cu(II) sites to produce an unusual bimetallic tetranuclear metal-oxide motif $\{Cu_2V_2O_5\}$. A curious feature of the structure is evident in the coordination mode adopted by the ethylenediphosphonate ligand which bridges four Cu(II) and two V(V) sites.

The network structure of **2** may be described as $\{(V_2O_5)(O_3PCH_2CH_2PO_3)\}_n^{2n-}$ chains linked by $\{CuO_3N_2\}$ sites into a two-dimensional layer. The linking of phosphorus and Cu(II) polyhedra produces $\{Cu_2P_2O_4\}$ eight-membered rings, exhibiting the common di-μ(O,O′) geometry. The network connectivity also produces the 22-membered ring $\{Cu_2V_4P_4O_8C_4\}$.

The structure of **2** contrasts with that of the previously described bipyridyl material, [Cu(2,2′-bpy)(VO)($O_3PCH_2CH_2PO_3$)], shown in Figure 4. In contrast to **1** and [Cu(2,2′-bpy)(VO)($O_3PCH_2PO_3$)(H_2O)], **2** and [Cu(2,2′-bpy)(VO)($O_3PCH_2CH_2PO_3$)] exhibit distinct formulations and different oxidation states for the vanadium centers. The V(IV) sites of [Cu(2,2′-bpy)(VO)($O_3PCH_2CH_2PO_3$)] are isolated; i.e., there are no V−O−V interactions. Furthermore, the network structure of the bipyridyl derivative is constructed exclusively of the V−P−O−C substructure. In a fashion similar to that described for [Cu(2,2′-bpy)(VO)($O_3PCH_2PO_3$)(H_2O)], the Cu(II) sites of [Cu(2,2′-bpy)(VO)($O_3PCH_2CH_2PO_3$)] decorate the surface of the layer and are not required to establish network connectivity. However, the most distinctive and significant features of the structure of **2** are the presence of the binuclear $\{V_2O_7\}$ building block and the V(V) oxidation state. While the members of the bipyridyl family of materials exhibit exclusively V(IV) sites, the phenanthroline compounds contain V(IV) sites in **1**, V(V) sites in **2** and mixed valence V(IV)/V(V) in **3** and **4**. Since the oxidation−reduction potentials for 2,2′-bipyridine and 1,10-phenanthroline in water are nearly identical[82] and the energies associated the LUMO's are similar, the rationale for the preference of the bpy system for the reduced V(IV) state is not obvious.

Extension of the tether length in [{Cu(phen)}$_2$(V_3O_5)($O_3PCH_2CH_2CH_2PO_3$)$_2$(H_2O)] (**3**) has profound structural consequences as illustrated in Figure 5. The two-dimensional

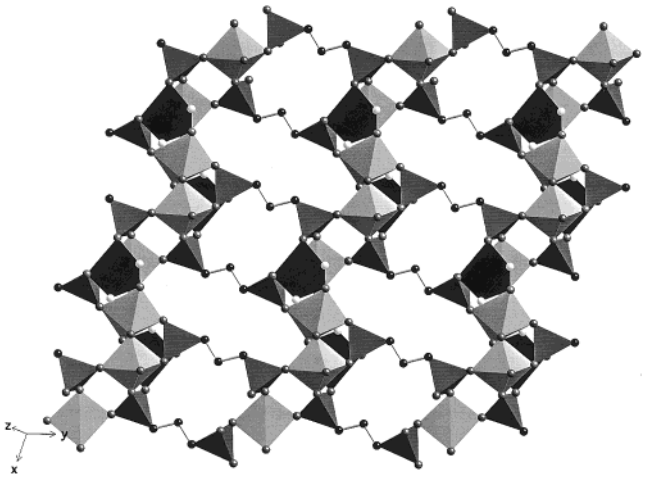

Figure 5. Polyhedral view of the network structure of [{Cu(phen)}$_2$(V_3O_5)($O_3PCH_2CH_2CH_2PO_3$)$_2$(H_2O)] (**3**).

structure of **3** is constructed from corner-sharing Cu(II) square pyramids, V(V) square pyramids, V(IV) octahedra, and phosphorus tetrahedra linked through the propylene bridges of the propylenediphosphonate ligands. The Cu(II) geometry is defined by two nitrogen atoms from the phenanthroline ligand and two oxygen donors from different organodiphosphonate ligands in the basal plane and a bridging oxo-group in the apical position. The octahedral vanadium site exhibits coordination to two trans disposed oxygen donors from different diphosphonate ligands, to two trans oxo-groups bridging to two neighboring V(V) sites, and an oxo-group and an aqua ligand bridging to the Cu(II) sites. The square pyramidal V(V) centers exhibit coordination to three oxygen donors from different diphosphonate ligands, a bridging oxo-group, and a terminal oxo-group. As a consequence, the structure of **3** is characterized by a trinuclear mixed valence V(IV)/V(V) cluster of corner-sharing polyhedra embedded within the two-dimensional network. Since the central V(IV) site also corner shares to two adjacent Cu(II) centers, an unusual pentanuclear bimetallic oxide subunit $\{Cu_2V_3O_5\}$ provides a building block for the network. Each propylenediphosphonate ligand links four vanadium and two copper sites, in contrast to the diphosphonate of **2** which bridge four copper and two vanadium sites.

The network may be described in terms of corner-sharing vanadium and phosphorus polyhedra linked by propylene bridges into a two-dimensional covalently linked layer. Alternatively, the layer may be described in terms of one-dimensional oxovanadium copper phosphate ribbons connected by propylene bridges into a layered structure. The network is characterized by a number of cyclic subunits, including the common $\{V_2P_2O_4\}$ ring with di-μ(O,O′) phosphate bridges. There is also a 16-membered cyclic substructure $\{V_2P_4O_4C_6\}$.

Several features of this structure are noteworthy. The detailed layer structure of **3** is quite distinct from that of **2**. While **2** exhibits a binuclear V(V) building block, compound **3** contains a trinuclear mixed valence subunit. Furthermore, the V−P−O−C substructure of **2** is one-dimensional, and network connectivity requires linking through the Cu(II) sites. In contrast, the V−P−O−C substructure of **3** is two-dimensional, with the $\{CuO_3N_2\}$ sites decorating the surfaces of the layer. Furthermore, while the structures of **2** and **3** are quite distinct, the bipyridyl counterparts [Cu(2,2′-bpy)(VO)($O_3PCH_2CH_2PO_3$)] and [Cu(2,2′-bpy)(VO)($O_3PCH_2CH_2CH_2PO_3$] are structurally analogous, differing primarily in the expansion of cyclic substructures of the layers as a consequence of carbon spacer lengthening.

(81) See, for example: Feng, P.; Bu, X.; Stucky, G. D. *Nature* **1997**, *388*, 735.

(82) Meites, L.; Zuman, P.; Rupp, E. B. *CRC Handbook Series in Organic Electrochemistry*; CRC Press Inc.: Boca Raton, FL, 1978; Vol. IV.

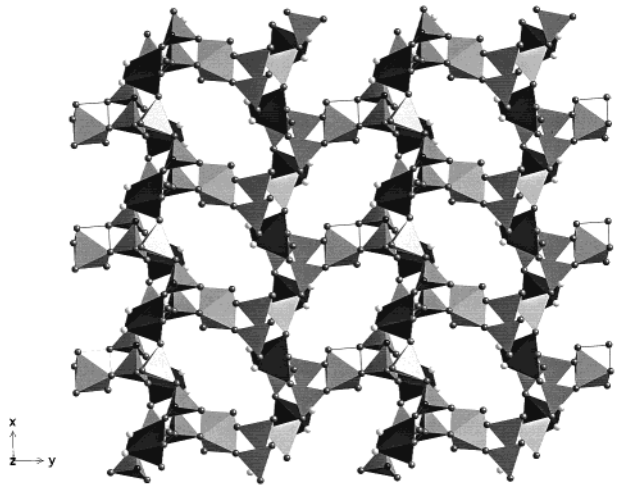

Figure 6. Polyhedral representation of the three-dimensional structure of $[\{Cu(phen)\}_2(V_3O_5)(O_3PCH_2PO_3)_2(H_2O)]$ (**4**), viewed normal to the *ab* plane.

Table 6. Summary of Magnetic Measurements

compd	paramagnetic ions[a]	C_{calc}[b] (emu K mol^{-1})	C_{obs} (emu K mol^{-1})	θ_{obs} (K)
1	Cu^{2+} (sp), V^{4+} (sp)	0.85	0.876(3)	−9.8(7)
2	Cu^{2+} (sp), Cu^{2+} (sp)	0.95	0.976(3)	−12.4(7)
3	Cu^{2+} (sp), Cu^{2+} (sp), V^{4+} (o)	1.32	1.200(1)	−2.2(2)
4	Cu^{2+} (sp), Cu^{2+} (sp), V^{4+} (o)	1.32	1.365(2)	−5.12(2)

[a] sp = square pyramidal; o = octahedral. [b] The Curie constant was determined using the Curie law $C = (Ng^2\mu_B^2S(S+1))/3k \approx (\mu_{eff}^2)/8$ where N is Avogadro's number, g the Landé splitting factor, μ_B the Bohr magneton, S the total spin quantum number. The values $g_{V^{4+}} = 2$, $g_{Cu^{2+}} = 2.25$ were assumed.

The most unusual characteristic of the phenanthroline system is the discovery of a three-dimensional structure. While **1**−**3** and the bipyridyl family share the common characteristics of two-dimensional structures, $[\{Cu(phen)\}_2(V_3O_5)(O_3PCH_2PO_3)_2(H_2O)]$ (**4**) exhibits a three-dimensional framework, shown in Figure 6. The structure of **4** is constructed from the corner-sharing of Cu(II) square pyramids, V(IV) octahedra, V(V) tetrahedra, and phosphorus tetrahedra. The Cu(II) site is defined by two nitrogen donors from the phenanthroline ligand and two oxygen atoms from a chelating methylenediphosphonate ligand, in the basal plane and a bridging oxo group from the tetrahedral vanadium site. The V(IV) center bonds to four oxygen donors from two chelating diphosphonate groups, a terminal oxo-group and an aqua ligand. This connectivity pattern requires the diphosphonate to bridge one Cu(II) site, one V(IV) site, and two V(V) sites.

The framework structure of **4** may be described in terms of $\{Cu(phen)(VO_2)(O_3PCH_2PO_3)\}_n^{2n-}$ layers linked by V(IV) octahedra into a three-dimensional structure. Alternatively, the structure consists of a three-dimensional $\{(V_3O_5)(O_3PCH_2PO_3)(H_2O)\}_n^{2n-}$ framework with $\{Cu(phen)\}^{2+}$ groups occupying channels running parallel to the crystallographic *a* axis.

Magnetic Properties. A summary of the results of the magnetic measurements is listed in Table 6. Figures 7−10 show the temperature dependence of the molar susceptibility (χ_m), inverse molar susceptibility ($\chi_m - 1$) and the $\chi_m T$ product for the entire series of oxovanadium organophosphonate phases with copper-phenanthroline building blocks in the temperature range 2−350 K. As shown in Table 6, compounds **1**−**4** contain the

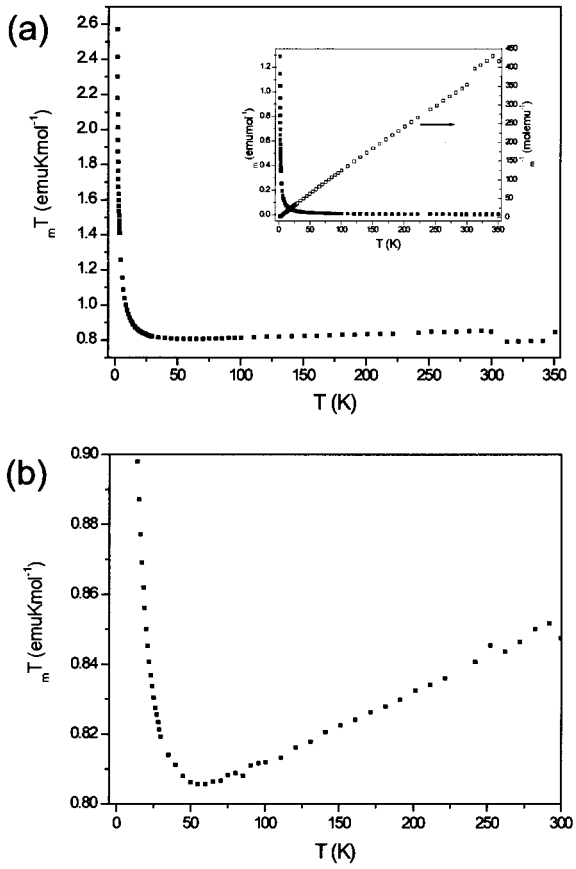

Figure 7. Temperature dependence of $\chi_m T$ for compound **2** between 2 and 350 K. Inset shows the ZFC magnetic susceptibility data.

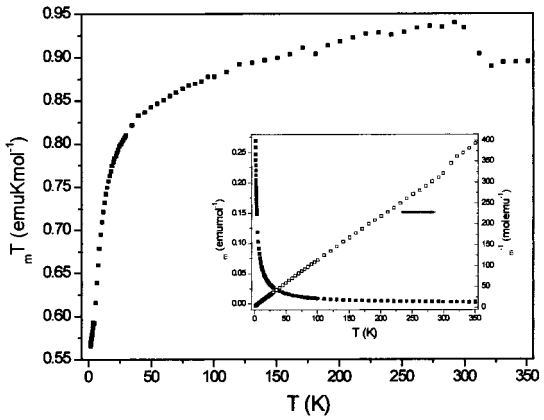

Figure 8. (a) Temperature dependence of $\chi_m T$ for compound **1** between 2 and 350 K. Inset shows the ZFC magnetic susceptibility data. (b) Minimum of $\chi_m T$.

paramagnetic ions Cu(II) (square pyramidal, $3d^9$) and/or V(IV) (square pyramidal or octahedral, $3d^1$); both are $S = 1/2$ magnetic centers. The χ_m vs T plots for all four compounds (Figures 7−10, insets) show typical Curie−Weiss behavior with no obvious signatures for even significant low-dimensional short-range correlations (i.e., broad maxima). To a good approximation, the high-temperature portion (>100 K) of the susceptibility data can be fitted to the Curie−Weiss law, $\chi = C/T - \theta$, where C is the Curie constant, T the temperature, and θ the Weiss constant. There is reasonable agreement between the experimental and theoretical Curie constants, calculated using common Landé splitting factors for the magnetic ions ($g_{V^{4+}} = 2$ and $g_{Cu^{2+}} = 2.25$). Overall, the behavior of these magnetically dilute compounds appears to be dominated by very weak antiferro-

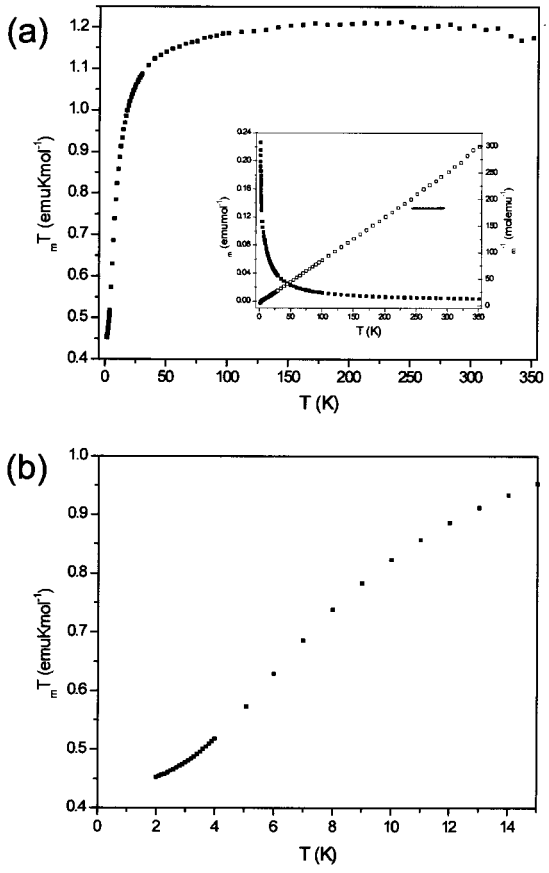

Figure 9. Temperature dependence of $\chi_m T$ for compound **4** between 2 and 350 K. Inset shows the ZFC magnetic susceptibility data.

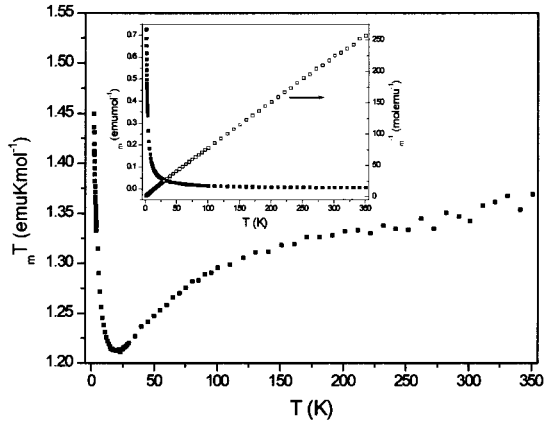

Figure 10. (a) Temperature dependence of $\chi_m T$ for compound **3** between 2 and 350 K. Inset shows the ZFC magnetic susceptibility data. (b) Low-temperature range showing a minimum of $\chi_{[0}T$.

magnetic interactions of the paramagnetic ions as indicated by the small negative θ values (Table 6). Further insight is provided by the $\chi_m T$ vs T plots (Figures 7−10).

As indicated previously, the $\{Cu(1)_2O_3N_2\}$ and $\{Cu(2)_2O_3N_2\}$ square pyramids in compound **2** serve to link zigzag chains of alternating V_2O_5 and $O_3PCH_2CH_2PO_3$ units into two-dimensional layers. Within these sheets, each Cu^{2+} ion is linked through a double oxo-bridge to a crystallographic equivalent to form approximate pairs that are 5.065 Å (Cu(1)−Cu(1)) and 5.105 Å (Cu(2)−Cu(2)) apart, respectively. Additionally, these Cu−Cu pairs are insulated from each other within (>8 Å) as well as between (>6.4 Å) the layers. Thus, one would most likely anticipate magnetic properties that are characteristic of binuclear cluster systems (i.e., Bleaney−Bowers type)[51,57,61,83] if there are significant interactions between neighboring Cu(II) ions. Figure 7 shows the temperature dependence of the molar susceptibility as well as $\chi_m T$ for compound **2**. It is clear that the magnetic behavior of $[\{Cu(phen)\}_2(V_2O_5)(O_3PCH_2CH_2PO_3)]$ is dominated by antiferromagnetic interactions, as indicated by the gradual decrease of the magnetic moment down to about 50 K followed by a rapid and sudden drop toward a singlet ground state. This observation is also consistent with a compensation of the two spin-1/2 sublattices upon onset of antiferromagnetic exchanges since the two Cu(II) ions are expected to have comparable Landé splitting factors (g) given their similar environments. Surprisingly, we do not observe a maximum in the susceptibility data down to 2 K even though $\theta = -12$ K. For a dimer magnetic system,[84] we would expect $T(\chi_{max})$ to be at approximately 20 K, but this is not reflected in the magnetic data, suggesting the presence of additional interactions between Cu(II) ions beyond the isolated binuclear regime such as interdimer or 3-D exchange interactions.

The magnetic behavior of compounds **1** and **4** is consistent with the fact that there are two different paramagnetic metal ions, Cu(II) and V(IV), with dissimilar g values. Not surprisingly, the magnetic susceptibility data show evidence for uncompensated moments at low temperatures, giving rise to characteristic low-dimensional ferrimagnetic behavior.[54−56,58−60,85−94] The structure of [Cu(phen)(VO)-$(O_3PCH_2PO_3)(H_2O)$] consists of square pyramids of $\{CuO_3N_2\}$ and $\{VO_5\}$ linked by the diphosphonate ligand $O_3PCH_2PO_3$ to form a two-dimensional structure. Intralayer metal−metal (Cu−Cu, Cu−V, and V−V) distances are in the range 5.043−6.419 Å so some interactions may be expected although the true magnetic dimensionality is not entirely clear. As shown in Figure 8a, a gradual decrease in the $\chi_m T$ product with decreasing temperature is followed by an abrupt increase at about 50 K. The shallow and rounded minimum at low temperature, emphasized in Figure 8b, is indicative of ferrimagnetic behavior in this compound. The source for the two-dimensional ferrimagnetic behavior can be assumed to be weak intralayer antiferromagnetic interactions between nearest neighbor metal ions. The absence of any transition in the susceptibility data at low temperature shows the lack of any long range ordering between the Cu/V layers. Similarly, the $\chi_m T$ vs T plot for compound **4** resembles one for a linear chain ferrimagnetic

(83) *Magnetochemistry;* Carlin, R. L., Ed.; Springer-Verlag: New York, 1986.
(84) For $S = 1/2$ binuclear clusters, $J_{12} = -1.247kT_c$ and $\theta = J_{12}/2k$, where J_{12} is the exchange interaction, k is the Boltzmann's constant, T_c is the critical temperature (corresponding to χ_{max} for antiferromagnetic interactions), and 0 is the Weiss constant. One can calculate the value of T_c if all other values are known.
(85) Qiang, X.; Darriet, J.; Soubeyroux, J. L.; Georges, R. *J. Magn. Magn. Mater.* **1988**, *74*, 219.
(86) Pei, Y.; Nakatani, K.; Kahn, O.; Sletten, J.; Renard, J. P. *Inorg. Chem.* **1989**, *28*, 3170.
(87) Sapiña, F.; Coronado, E.; Gomez-Romero, P.; Beltran, D.; Burriel, R.; Carlin, R. L. *J. Appl. Phys.* **1990**, *67*, 6003.
(88) Coronado, E.; Gómez-García, C. J.; Borrás-Almenar, J. J. *J. Appl. Phys.* **1990**, *67*, 6009.
(89) Fabretti, A. C.; Giusti, A.; Albano, V. G.; Castellari, C.; Gatteschi, D.; Sessoli, R. *J. Chem. Soc., Dalton Trans.* **1991**, 2133.
(90) Stumpf. H. O.; Pei, Y.; Ouahab, L.; Berre, F. L.; Codjovi, E.; Kahn, O. *Inorg. Chem.* **1993**, *32*, 5687.
(91) Ruiz, R.; Surville-Barland, C.; Journaux, Y.; Colin, J. C.; Castro, I.; Cervera, B.; Julve, M.; LLoret, F.; Sapiña, F. *Chem. Mater.* **1997**, *9*, 201.
(92) Escuer, A.; Vicente, R.; Fallah, M. S. El; Goher, M. A. S.; Mautner, F. A. *Inorg. Chem.* **1998**, *37*, 4466.
(93) Chiozzone, R.; González, R.; Kremer, C.; Munno, G. D.; Cano, J.; Lloret, F.; Julve, M.; Faus, J. *Inorg. Chem.* **1999**, *38*, 4745.
(94) Ruiz-Pérez, C.; Sanchiz, J.; Hernández-Molina, M.; Lloret, F.; Julve, M. *Inorg. Chim. Acta* **2000**, *298*, 202.

system with intrachain antiferromagnetic coupling between nearest neighbor, as shown in Figure 9, which displays a steady decay of the moment from room temperature to about 20 K where there is a prominent and rounded minimum before the moment rapidly increases at low temperature. Structurally, [{Cu(phen)}$_2$(V_3O_5)($O_3PCH_2PO_3$)$_2$(H_2O)] exhibits a three-dimensional framework constructed from corner-sharing of Cu(II) square pyramids, V(IV) octahedra, V(V) tetrahedra, and $O_3PCH_2PO_3$ building blocks. Magnetically, there are local linear arrangements of Cu(II) (sp)-V(IV) (o)-Cu(II) (sp) (sp = square pyramidal; o = octahedral) moeities which are separated by the $O_3PCH_2PO_3$ units. The Cu−V separations within these linear magnetic trimers are 4.581 and 4.984 Å. Since the shortest intertrimer distance is >7 Å, compound **4** appears to be a ferrimagnetic trimer system. However, the dimensionality of the magnetic lattices in **4** is also definitive since intertrimer Cu(II) interactions may still occur through the intervening oxo bridges.

Unexpectedly, compound **3** does not exhibit the anticipated ferrimagnetic behavior as seen in the previous two examples despite containing both Cu(II) and V(IV) metal ions. As shown in Figure 10a, its magnetic behavior appears to be dominated by antiferromagnetic coupling but the exchange is the weakest of the series as indicated by the relatively small θ value (−2.2(2) K). Therefore, we do not see manifestation of uncompensated spin lattices above 2 K as observed in compounds **1** and **4**. Interestingly, a closer inspection of the low temperature $\chi_m T$ product (Figure 10b) does show the beginning of a very shallow minimum, suggestive of antiferromagnetic coupling between the Cu(II) and V(IV) ions leading to overall ferrimagnetic behavior below 2 K owing to different g factors between the two metal ions. The magnetic structure within the overall two-dimensional layered network of [{Cu(phen)}$_2$(V_3O_5)($O_3PCH_2CH_2CH_2PO_3$)$_2$(H_2O)] consists of Cu(II)−V(IV)−Cu(II) linear trimers with substantially close intratrimer Cu−V separations of 3.503 and 4.377 Å. These trinuclear clusters are fairly well isolated, magnetically, as shown by the closest intertrimer distance of 9.436 Å within a network layer and 5.936 Å between layers. The overall antiferromagnetic feature in the $\chi_m T$ vs T plot suggests that the g values of Cu and V ions in this compound are fairly close, thereby rendering the magnetism to be best modeled by an isolated $S = 1/2$ linear trimer system;[61] however, the extremely weak nature of the antiferromagnetic coupling and the presence of a residual moment at low-temperature preclude any fitting to a model.

Conclusions

Hydrothermal synthesis has allowed the preparation of a new series of organic−inorganic materials of the oxovanadium/organophosphonate/M(II)−organoimine family. While [Cu(phen)(VO)($O_3PCH_2PO_3$)(H_2O)] (**1**), [{Cu(phen)}$_2$(V_2O_5)($O_3PCH_2CH_2PO_3$)] (**2**), and [{Cu(phen)}$_2$(V_3O_5)($O_3PCH_2CH_2CH_2PO_3$)] (**3**) exhibit two-dimensional structures; [{Cu(phen)}$_2$(V_3O_5)($O_3PCH_2PO_3$)$_2$(H_2O)] (**4**) is three-dimensional. The hybrid materials exhibit a range of magnetic properties, reflecting the presence of a single type of paramagnetic metal ion Cu(II) in **1** and two distinct paramagnetic ions Cu(II) and V(IV) in **2**−**4.**

Acknowledgment. The work at Syracuse University was supported by a grant from the National Science Foundation, CHE 9987471.

Supporting Information Available: X-ray crystallographic files, in CIF format, for **1**−**4**. Views of the metal−ligand environments of **1**−**4**, showing the atom-labeling schemes and the anisotropic thermal parameters. This material is available free of charge via the Internet at http://pubs.acs.org

IC010186I